Dissociative Electron Attachment to Gas- and Condensed-Phase CF_3Cl: Anion Desorption and Trapping

Fritz Weik* and Eugen Illenberger

Institut für Physikalische und Theoretische Chemie, Freie Universität Berlin, Takustrasse 3, D-14195 Berlin, FRG

Kannadaguli Nagesha and Léon Sanche

Groupe du Conseil de Recherches Médicales en Sciences des Radiations, Faculté de Médecine, Université de Sherbrooke, Sherbrooke, Québec, Canada J1H 5N4

Received: August 4, 1997; In Final Form: November 5, 1997

The interaction of electrons in the energy range from near zero to 10 eV with CF_3Cl physisorbed on a Kr surface is studied and compared with previous gas-phase experiments on isolated molecules and CF_3Cl clusters. In the gas phase CF_3Cl shows resonances in the dissociative attachment (DA) cross section at 1.4 eV, near 4−5 eV, and at 9 eV with the 1.4 eV feature assigned as a single particle resonance with a strong C−Cl repulsive nature. From adsorbed CF_3Cl, we observe desorption of Cl^- and F^- with resonances in the cross section which can be correlated to the gas-phase DA features. Despite its antibonding nature, Cl^- desorption via the single particle resonance is very weak, indicating that *direct* desorption processes do not occur; i.e., orientations of the molecule with the C−Cl axis pointing away from the surface can be excluded, and desorption is always preceded by postdissociation interactions. Charge trapping is virtually restricted to the low-energy resonance. Its maximum is at 0.8 eV and reflects the energy shift of the transient ion due to solvation. The absolute trapping cross section is 43×10^{-18} cm^2, exceeding the gas-phase DA value by about 1 order of magnitude. The behavior of the low-energy resonance is described in terms of one-dimensional potential energy curves previously used to model temperature effects in DA to gas-phase CF_3Cl, with the anionic curve shifted by the solvation energy. It is shown that autodetachment, which is by far the dominant decay channel in the gas phase, is substantially suppressed in the condensed phase.

Introduction

The interaction of low-energy electrons with matter at different degrees of aggregation leading to negative ions gives insight into solvation processes. In the case of small molecules, diatomics and those that can be treated approximately like diatomics, electron attachment can be treated in accordance with the Franck−Condon principle. The transition and the subsequent dissociation of the transient anion can then be described using neutral and anionic potential energy curves evaluated in the framework of the Born−Oppenheimer approximation. If mass spectrometric techniques are applied, the observed signal corresponds to anionic molecules or anionic fragments. Data on neutral species involved in the process are still rare because there is no general and easy procedure to identify and detect them as is the case for ions. In gas-phase experiments, negative ions formed upon (dissociative) electron capture can be detected directly, thus allowing insight into decomposition processes of an isolated molecular anion. In the condensed phase, on the other hand, ions that do not gain sufficient kinetic energy to overcome the polarization barrier are trapped at the surface, resulting in charging of the film. From the rate of this charging the electron attachment coefficient can be calculated. This coefficient refers to attachment processes including those not seen in the ion desorption experiment. Thus, the data from desorption in combination with film charging can be compared with gas-phase data in order to obtain information on the change in reactivity in the different environments.

Recently, efforts have been made in order to understand the behavior of DA in different environments by employing simple diatomic molecules such as the oxygen and more complex molecules such as halogenated methane, which are of special interest because of their potential to destroy the stratospheric ozone layer. In these studies, complementary information from desorption and charging experiments in the condensed phase[1−3] were combined while comparing with the gas-phase data.[4,5] In general, DA cross sections were found to be enhanced in the condensed phase, in certain cases dramatically as in the case of CH_3Cl.[6,7]

The present work focuses on CF_3Cl for which gas-phase data exist on electron scattering[8,9] and DA,[10] including the temperature dependence giving insight into the dynamics of the fragmentation process at low electron energies.[11] Various DA channels[12] have been observed, the lowest of which is a single particle resonance that exclusively dissociates to Cl^-.[13] Absolute DA cross sections were published by Underwood-Lemons et al.[14] The observed effects have been modeled by means of diatomic like potential energy curves which is justified by the pronounced impulsive character of the dissociation along the C−Cl axis.[11,15] The model explains the balance between two competing processes: the dissociation of the molecule after electron attachment and the emission of the electron before fragmentation (referred to as autodetachment). This latter process is seen in scattering experiments by detecting the electron. With this information, CF_3Cl^- may serve as a model

S1089-5647(97)02535-2 CCC: $15.00
Published on Web 01/29/1998

system for studying the effects of condensation on the two competing decay channels.

In this contribution we present data on ion desorption from condensed CF_3Cl as well as absolute attachment cross sections. These results are compared with previous experiments on gas-phase CF_3Cl.

Experimental Section

This study was performed with two different experimental arrangements. The desorption experiments were carried out in the Berlin laboratory while the charging data were obtained in the Sherbrooke laboratory. Both laboratories use similar techniques for generation of the electron beam and preparation of the condensed-phase samples.

A. The Desorption Apparatus. The experimental setup was described earlier in detail;[16,17] only a brief description is provided in this section.

It consists of a UHV chamber evacuated with a turbo molecular pumping system and an ion getter pump reaching a base pressure of 5×10^{-10} mbar.

The CF_3Cl/Kr films were condensed onto a polycrystalline Pt substrate mounted on a UHV manipulator. The sample is electrically insulated and can be translated along the three Cartesian coordinates and rotated around its axis. The crystal mounting is cooled via a copper-braced connection to the cold head of a closed cycle He cryostat. The temperature of the substrate is 25 K. The film is evaporated by heating the crystal to several hundred degrees kelvin.

Film dosing is performed by placing the crystal in front of a capillary at a distance of 8 mm and expanding a calibrated volume of the gas into the UHV system. The film thickness is derived from that volume and the absolute gas pressure measured by a "Baratron" manometer. The calibration of a monolayer is possible by thermal desorption spectra discriminating between the multilayer and monolayer peaks. These desorption spectra are recorded with a residual gas analyzer. The amount of expanded gas for the monolayer deposition is then determined by the Baratron. We estimate the accuracy of the dosing procedure to be 20%.

The electron source is a trochoidal electron monochromator introduced by Stamatovic and Schulz.[18] It uses a crossed electric and magnetic field for the dispersion of the electron energy distribution emitted from the filament. Outside the dispersion region the magnetic field aligns the electrons, thus generating a collimated electron beam with sufficient intensity down to thermal electron energies. The intensity of the electron beam that strikes the target is measured using a nanoamperemeter. The electron energy is calibrated with respect to the vacuum level by the sharp onset of the electron current at the substrate. Typical resolution is 200 meV at a current of 40 nA; the uncertainty in energy is 50 meV.

Desorbing anions are extracted and focused into a quadrupole mass filter equipped with a commercial ion lens system. The axis of the mass filter is aligned perpendicular to the electron beam. After traversing through the filter the ions are detected by a secondary electron multiplier and counted with a multichannel scaling connected to a personal computer. The ion signal is maximized by adjusting the angle of the crystal with respect to the fixed axis of the electron beam and the quadrupole.

All desorption spectra are obtained from a submonolayer amount of CF_3Cl molecules adsorbed on a 15 monolayer (ML) Kr spacer. With a 15 ML rare gas spacer the interaction of a charge (on its surface) with the metallic substrate can be neglected.

B. Charge Trapping Measurements. As in the previous section, we give here only a brief overview of the experiment which is described in detail elsewhere.[19] The apparatus is housed in a UHV chamber pumped with an ion getter pump and a cold head of a closed cycle He cryostat acting as a cryopump.

The substrate in this apparatus is a polycrystalline Pt foil mounted onto the cold head of a second closed cycle He cryostat. The temperature of the Pt foil is held at 23 K during the measurements. A magnetically collimated monochromatic electron beam (fwhm $\approx$ 40 meV) of variable energy impinges onto the crystal surface at normal incidence. As in the desorption experiments, CF_3Cl is adsorbed on a Kr film acting as spacer to the metallic substrate. After the charging measurements, the Pt foil is resistively heated in order to evaporate the film. The dosing procedure is similar to that of the desorption experiment. Monolayer calibration was obtained by the observation of interference structures created by the incident electrons in the sample current.[20] The accuracy of the dosing is estimated to be 20%. Energy calibration was performed as in the desorption experiment.

The film is charged by setting the electron beam to the desired energy for a defined time, so that the total amount of charges impinging on the film is known. Immediately afterward, the onset of electron transmission to the substrate is scanned. If charging has occurred, the electrons impinging on the film are subjected to a retarding potential due to the accumulated charge; this results in an energy shift of the onset. The charging coefficient A_s can be calculated[19] according to

$$A_s(E) = \frac{d}{dt}\Delta V(t)|_{t\to 0} = \frac{\rho_0 J_0 L \mu_{CT}(E)}{\kappa \epsilon_0} \qquad (1)$$

A_s is the time derivative of the onset curve shift ΔV in the limit $t \to 0$. ρ_0 denotes the average surface density of the CF_3Cl molecules, J_0 the current density, L the film thickness, μ_{CT} the trapping cross section of the electrons, κ the dielectric constant, and ϵ_0 the vacuum permittivity. $A_s(E)$ is obtained by monitoring small shifts in the onset of the electron transmission ($\Delta V < 50$ meV) corresponding to small bombardment time at different electron energies;[19] μ_{CT} is determined from eq 1. The absolute and relative uncertainty on μ_{CT} are estimated to be 50% and 10%, respectively.

The charging experiment is limited to energies below the exciton level of the Kr film. The lowest excitonic state at the surface is located at 9.95 eV.[21] Electrons with energies above the exciton level will be scattered to lower energies and then contribute to the charging of the film.

Results

A. Review of Previous Gas-Phase Experiments. Figure 1 shows a reproduction of the excitation functions of the fragments Cl^- and F^- previously obtained under single collision conditions in the Berlin laboratory.[12] It exhibits three resonance features associated with DA: one at 1.4 eV, a second one in the energy range 4−5 eV, and a third one as a very small contribution at 9 eV.

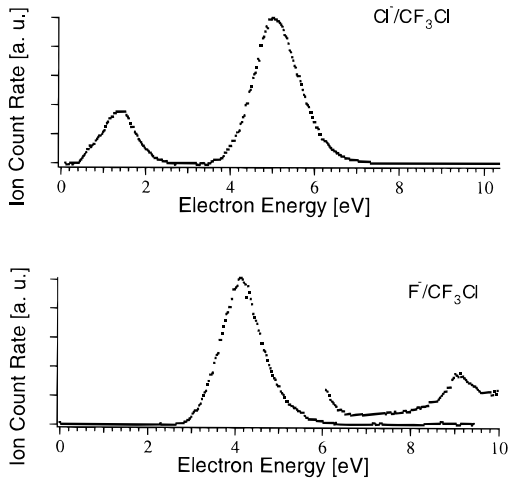

Figure 1. Relative DA cross sections for Cl^- and F^- formation in gas-phase CF_3Cl under single-collision conditions; adapted from ref 12.

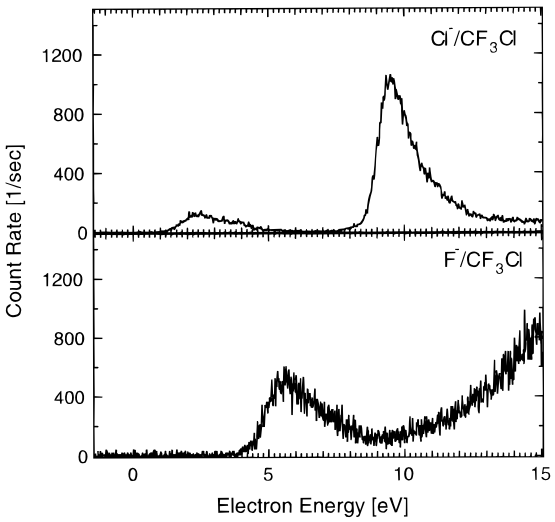

Figure 2. Desorption of Cl^- and F^- from a 0.3 monolayer CF_3Cl on a 15 monolayer Kr film which act as a spacer to the metallic substrate. The Cl^- spectrum is an average over eight scans.

The low-energy resonance is exclusively associated with Cl^- formation according to the reaction

$$e^- + CF_3Cl \rightarrow CF_3Cl^- (1.4\ eV) \rightarrow Cl^- + CF_3 \qquad (2)$$

This electronic state is assigned as single particle resonance[22] having a distinct C−Cl repulsive nature as seen, for example, in the high translational energy release to the two dissociation products.

For the second resonance the situation is less straightforward: under collision-free conditions the following ionic fragments appear (the numbers in parentheses refer to the peak position and relative intensity, respectively): Cl^- (4.8 eV/100), F^- (4.1 eV/50), FCl^- (4.0 eV/20), CF_2Cl^- (4.1 eV/10), and CF_3^- (3.7 eV/0.5).[10,12] In Figure 1, we show only the atomic fragments Cl^- and F^-, relevant in the desorption experiment. TOF measurements[12] showed that all fragment ions from the second resonance appear with low kinetic energy, indicating no particular valence character of this electronic state.

From electron impact measurements, it has been suggested that the breaking of the C−F bond is the main process leaving an excited CF_2Cl^- fragment[23,24] which may further decompose into Cl^-, F^-, and CF^- .[23] This picture is supported by the gas-phase DA data showing a weak CF_2Cl^- signal concentrated at the lower energy part of the second resonance.[10] If more energy is brought into the molecule, further fragmentation of CF_2Cl^{*-} is the dominant reaction path. In fact, while no CF_2Cl^- intensity is seen for energies above 5 eV, the resonance profiles of the fragments Cl^-, F^-, and FCl^- extend to about 6 eV.[10] We may thus conclude that this second feature is a core excited resonance correlating with electronically excited CF_2Cl^{*-}, which further decays according to

$$CF_3Cl^{*-} (4.8\ eV) \rightarrow CF_2Cl^{*-} + F \rightarrow CFCl + F^- + F \qquad (3a)$$

$$\rightarrow Cl^- + CF_3 \qquad (3b)$$

$$\rightarrow FCl^- + CF_2 \qquad (3c)$$

Since the known electronically excited neutral states (including spin-forbidden triplet states) are considerably above the energy of this resonance,[23] it is most likely of the Feshbach type. The F^- TOF profile exhibits a remarkable asymmetry toward higher flight times which is an indication of a metastable decay occurring in the microsecond domain, which also supports the above decomposition scheme. Further, there is obviously a weak correlation of this Feshbach resonance directly to the ground-state fragments CF_3^- + Cl as documented by the weak CF_3^- intensity.

One remarkable feature of DA to gas-phase CF_3Cl should be noted: the Cl^- intensity from the low-energy resonance (at 1.4 eV) is considerably smaller than that from the second resonance (at 4.8 eV) (see Figure 1). On the other hand, from elementary considerations,[22] the electron attachment cross section increases with decreasing electron energy. The low Cl^- intensity at 1.4 eV is the result of the smaller survival probability of the CF_3Cl^- single particle resonance owing to a strong electron autodetachment.

Near 10 eV a very weak Cl^- and F^- signal is seen (Figure 1). The VUV absorption spectrum obtained with synchrotron radiation shows a dominant peak at 9.6 eV with a maximum cross section of 40×10^{-18} cm^2.[25] Another VUV work with a discharge tube as light source gives a prominent peak at 9.7 eV.[26] This feature was assigned to the 3s Cl lone pair → Rydberg transition. It is thus likely that the negative ion state near 9 eV can be described as a two particle−one hole resonance associated with the Rydberg excited neutral state.

B. Ion Desorption and Charge Trapping in Condensed CF_3Cl. In Figure 2, the desorption spectra from a submonolayer CF_3Cl adsorbed on a multilayer Kr spacer film are plotted. While DA to gas-phase CF_3Cl results in a variety of ionic fragments, desorption from condensed CF_3Cl is restricted to the ionic fragments F^- and Cl^-. The ion yield curve shows pronounced resonances, indicating that desorption of F^- and Cl^- is driven by the DA mechanism.

In general, desorption of an ionic fragment via DA can be pictured on a molecular site by including the solvation energy of the negative charge due to the electronic polarization interaction with its environment; i.e., the resonance (or the attachment energy) is lowered with respect to the gas phase. Desorption of ionic fragments, on the other hand, is subjected to energetic and structural constraints that may modify considerably the energy of the desorption structure with respect to the attachment energy. From an energy point of view, only those DA reactions that release sufficient kinetic energy to the ionic fragment to overcome the polarization barrier can contribute to desorption. From the structural point of view, it is clear that

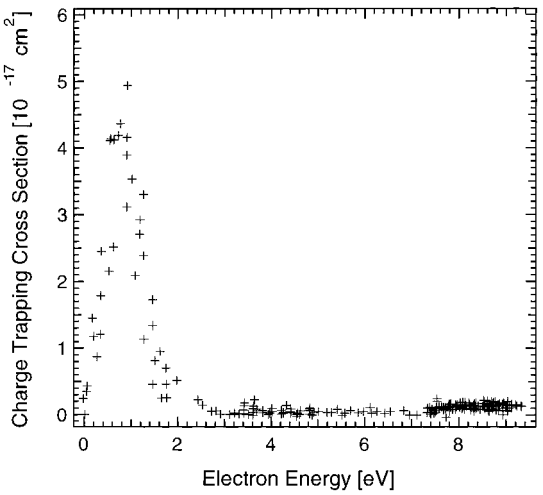

Figure 3. Charge trapping cross section of a 0.1 monolayer CF_3Cl on a 15 monolayer Kr film.

an *impulsive* dissociation process with the axis parallel to the surface normal and the ionic fragment pointing away from the surface is the ideal situation for a direct desorption process. Otherwise, energy transfer via *postdissociation interactions* may eventually prevent the ion from desorption or shift the desorption resonance to higher energies.

As mentioned above, the single particle resonance at 1.4 eV is strongly repulsive, leading to fast Cl^- ions in the gas phase with energies exceeding 1.0 eV for electron energies above 1.5 eV.[13] As can be seen from Figure 2, the Cl^- desorption intensity in the vicinity of the single particle resonance is fairly low. We estimate this intensity to be 2−3 orders of magnitude lower than F^- desorption from condensed CF_4.[27] In the gas phase, CF_4^- yields energetic F^- ions with kinetic energies in the range between 0.7 and 1.5 eV[27] and thus comparable to the present system Cl^-/CF_3Cl. We therefore suggest that direct desorption does not occur; i.e., orientations of the molecule with the C−Cl axis pointing away from the surface can be excluded.

Interestingly, in the vicinity of the second gas-phase resonance (4−5 eV) we exclusively observe F^- desorption with a resonance maximum at 5.5 eV. In the gas phase the decomposition of this electronically excited precursor ion was explained by a sequential dissociation with the cleavage of a C−F bond as the first step. Accordingly, the 9 eV gas-phase resonance (leading to a very low F^- and Cl^- intensity), most likely associated with a Cl lone pair → Rydberg transition, exclusively results in a strong Cl^- desorption resonance. The continuous increase of the F^- desorption signal above 10 eV is most likely due to electronic excitation of the neutral molecule leading to dipolar dissociation into $F^- + CF_2Cl^+$.

Figure 3 shows the cross section for charge trapping by a submonolayer of CF_3Cl on a 15 ML Kr spacer. The trapping cross section was calculated according to eq 1 with $\kappa = 1.91$ for solid Kr.[28] The cross section peaks at 0.8 eV with a value 43×10^{-18} cm^2. For comparison, the gas-phase DA cross section from a beam experiment is 3.9×10^{-18} cm^2,[14] and the resonant contribution in the total scattering cross section at (2.0 eV) $\approx 18 \times 10^{-16}$ cm^2.[9]

Figure 3 indicates that the charge trapping cross section is dominated by the low-energy resonance while at higher energies the signal is only slightly above the detection limit ($\approx 1 \times 10^{-18}$ cm^2). We accumulated a large number of data points from several film samples in order to clarify the situation near 4 and 8 eV.

Since $\mu_{CT}(E)$ is nonzero near zero energy (see Figure 3), the measurement of the onset of the electron transmission spectrum itself can contribute to charge trapping. We minimized its contribution to the data of Figure 3 by monitoring the shift of the onset in extremely short time (e.g., 25 ms) compared to the electron bombardment time (e.g., 2 s). The uncertainty in the energy and the charge density was minimized by limiting the overall potential to <50 meV.[19]

In our determination of $\mu_{CT}(E)$ we must also consider that the measured cross section corresponds only to anions that remain on the Kr film surface. However, Figure 2 shows that for energies above ≈2 eV the intensity of anions that escape into vacuum is not negligible. Consequently, $\mu_{CT}(E)$ cannot be equated to a total *stable anion formation* (SAF) cross section, $\mu_{SAF}(E)$ above ≈2 eV. Thus, for those energies $\mu_{CT}(E)$ gives only a lower limit to the SAF cross section. Since anion desorption is negligible for energies below ≈2 eV in the present experiments, $\mu_{CT}(E) = \mu_{SAF}(E)$ in the results of Figure 3. Furthermore, $\mu_{SAF}(E)$ should correspond exclusively to a DA cross section $\mu_{DA}(E)$ since stabilization of isolated CF_3Cl^- is not possible from a transition in the Franck−Condon region.

The resonant nature of the charge trapping cross section around 0.8 eV indicates that the trapping proceeds predominantly via the low-energy single particle resonance. The extra charge is then localized on the DA fragment Cl^- or on the stabilized parent anion CF_3Cl^-. Attachment experiments to neutral CF_3Cl clusters, in fact, have demonstrated[22] that a considerable amount of undissociated ions $(CF_3Cl)_n^-$, $n \geq 1$, are formed in addition to the DA products $Cl^-\cdot(CF_3Cl)_n$, $n \geq 0$. These experiments have further demonstrated that attachment via this low-energy state is substantially enhanced in clusters due to reduced autodetachment.

The observation of the enhancement in DA cross sections in the cluster experiments has recently been corroborated with measurements on charge trapping by CF_3Cl molecules embedded into the bulk of a solid Kr film.[29] They indicate that the DA cross section is enhanced by a factor of 3 from the surface value as expected from the increase in polarization energy in going from surface to bulk Kr. Based on the cluster results, it has been suggested that, besides DA, electron attachment to CF_3Cl within a solid lattice also leads to CF_3Cl^- stabilized by the caging effect of the neighboring molecules. Thus, all condensed-phase experiments indicate that the autodetachment channel of the low-energy resonance is markedly suppressed upon condensation.

It is also important to note that the charge trapping cross section of the low-energy resonance depends on the Kr spacer film thickness for small thicknesses. This is illustrated in Figure 4 where the dependence of the maximum in the charge trapping cross section at ≈0.8 eV for CF_3Cl is plotted as a function of Kr spacer film thickness L. The charge trapping cross section gradually increases and becomes nearly constant at large L. The decrease in μ_{SAF} for small L has been observed earlier for CH_3Cl adsorbed at the Kr surface.[7] This pronounced decrease in the cross section can be understood to be due to the proximity of the metal substrate.

C. Discussion of the Low-Energy Single Particle Resonance. As mentioned above, DA into $CF_3 + Cl^-$ at low energy proceeds through a single particle resonance followed by direct electronic dissociation along a repulsive surface with virtually all of the excess energy released as translational energy into the two products. We have thus an *impulsive* dissociation where CF_3 behaves as a "rigid" radical which justifies the description

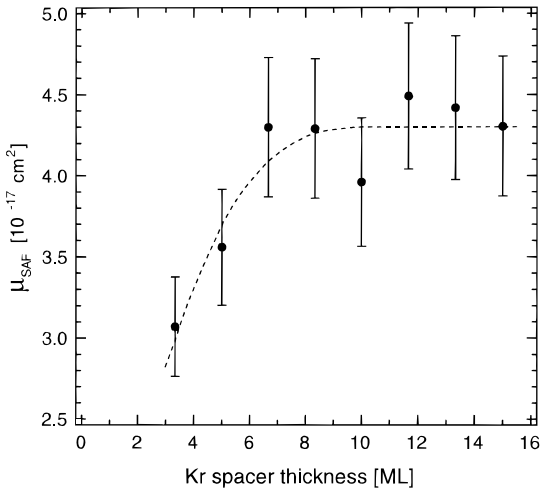

Figure 4. Dependence on Kr layer thickness of the maximum in the charge trapping cross section around 0.8 eV shown in Figure 3. The dotted curve is a guide to the eye.

of the process in terms of one-dimensional potential energy curves with R(C−Cl) as the relevant internuclear distance.

A quantum mechanical theory of DA to diatomic molecules has been developed three decades ago by O'Malley[30] in the framework of adiabatic potential energy curves. Nonadiabatic coupling mechanisms in DA have been treated by Domcke.[31] More recently, an instructive classical model of DA was developed by Lehr and Miller[15] and Lehr,[32] based on the classical theory of Penning ionization.[33] DA can be viewed as the reverse of Penning ionization with one more electron in the system. This model was able to quantitatively describe the observed temperature effects in DA to gas-phase CF_3Cl.[11,15,32] We will use these model potentials and parameters to discuss DA to physisorbed CF_3Cl.

Generally, the cross section for dissociative attachment, μ_{DA}, can be written as a product of the attachment cross section, μ_0, and the "survival probability" P

$$\mu_{DA} = \mu_0 P \tag{4}$$

where P expresses the probability that the anionic system survives dissociation with respect to autodetachment.

In the framework of adiabatic potential energy curves and assuming a Franck−Condon transition from the neutral to the repulsive anionic potential energy curve, the survival probability can be expressed as

$$P(E) = \exp\left(-\int_{R_E}^{R_c} \frac{\Gamma(R)\,\mathrm{d}R}{\hbar v(R)}\right) \tag{5}$$

with R_E the internuclear distance where the electronic transition occurs, R_c the crossing point between the ground-state neutral and anion potential energy curves, $v(R)$ the radial velocity between the dissociating fragments, and $\Gamma(R)$ the autodetachment width. Γ is related to the autodetachment lifetime by $\tau_{AD} = \hbar/\Gamma$. Expression 5 for P is the result of both the quantum mechanical[30] and the classical approach.[15]

The shape of the attachment cross section μ_0 can be approximated using the reflection principle which is applicable to bound → free transitions.[34,35] It states that the Franck−Condon factors as a function of E for the electronic transition are given by reflecting the square of the vibrational wave function of the neutral state at the anionic potential energy curve.

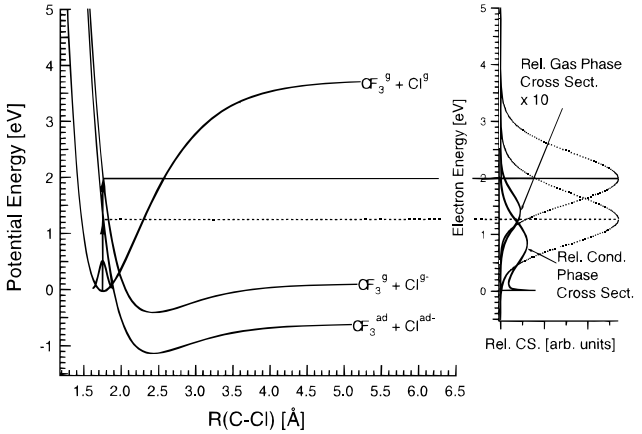

Figure 5. Illustration of the reflection principle in DA to CF_3Cl. The gas-phase potentials are Morse potentials taken from ref 32. The ionic condensed-phase curve is shifted by 0.72 eV (see text). Projections of the vibrational probability densities (dotted) and relative cross sections (solid). The index (ad) and (g) refers to the respective fragment at the surface and in the gas phase, respectively.

In Figure 5 we show the potential energy curves relevant for DA to gas-phase and condensed-phase CF_3Cl. The neutral and upper anionic curves are Morse potentials which were used to describe the temperature effects in DA to gas-phase CF_3Cl.[15,32] The experimental observations could be explained by fitting the autodetachment width $\Gamma(R)$ and using Boltzmann-weighted vibrational wave functions. For Γ exponential functions were used in the way that $\Gamma(E)$ increases exponentially with electron energy E.

Figure 5 also shows the reflection of the $v = 0$ probability density at the anionic gas-phase potential energy curve having a maximum at 2.0 eV and extending to about 3.5 eV. The energy position corresponds to the single particle resonance seen in the total[8] and inelastic scattering cross section.[9]

The gas-phase DA cross section, on the other hand, peaks at 1.4 eV and extends to about 2.2 eV.[22] This shift is a consequence of the exponential dependence of the survival probability on R (shown in Figure 5) and the exponentially increasing autodetachment width $\Gamma(E)$ as a function of E. These factors make DA from transitions at low energy (large intermolecular distance) more probable and increase the survival probability at low energy. In the gas phase, DA competes strongly with electron autodetachment. From the absolute values of the cross sections from electron beam experiments, i.e., resonant component of the total scattering cross section ≈18 × 10^{-16} cm^2,[8] DA cross section $\mu_{DA} = 3.9 \times 10^{-18}$ cm^2, [14] and the branching ratio between autodetachment and DA becomes $\mu_{AD}/\mu_{DA} \approx 462$.

Figure 5 also shows the potential energy curve for CF_3Cl^- physisorbed on the Kr surface with a downshift of 0.72 eV with respect to the gas-phase anion. This downshift corresponds to the surface polarization energy of a Kr film on the transient negative ion taken from experimental data.[28]

On the right-hand side of Figure 5 we show the projections of the ground-state probability function from gas phase (upper dotted curve) and condensed phase (lower dotted curve). The straight lines show the construction of this projection from the ground-state potential. The solid curves show the calculated relative cross section of the gas phase (upper trace) which peaks at 1.4 eV and the calculated relative cross section of the condensed phase (lower trace) peaking at 0.85 eV. These calculations were obtained by using eqs 4 and 5 for the survival probability and taking the R dependence in $\Gamma(R)$ from Lehr[32]

and Lehr and Miller[15] for the gas phase. For the condensed phase we used a $\Gamma(R)$ adjusted to the shift of the crossing point R_c since for distances larger than the crossing point, autodetachment no longer can occur, i.e., $\Gamma(R_c) = 0$. These calculations yielded an enhancement factor (i.e., the ratio of the peak maxima) of 14 for the survival probability of the fragment molecular ion, while the experiment gives an enhancement factor of about 11. One should note that the charging spectrum from Figure 3 shows the accumulated charge on the film without distinguishing whether this charge is localized on a stabilized molecular anion or on a fragmented Cl^- anion. The present model calculation also does not distinguish between the fragmentation and stabilization processes. It only calculates a relative cross section for forming an anionic entity with the excess charge in a bound state without considering the further fate of the system beyond the crossing point R_c. The peak at energies near zero in the condensed-phase theoretical curve of Figure 5 is due to the fact that we adopted O'Malley's formula, which tacitly assumes that the resonance state is purely repulsive and is situated higher than thermal energies. Such quantum mechanical threshold behavior holds in exceptional cases in accordance with Wigner's formalism,[36] as for some halides[37] where DA is exothermic. In our case, it should be noted that the transition energy in the Franck−Condon region is larger than the energy corresponding to R_c of the neutral CF_3Cl ground state. In addition, μ_0 in eq 4 is evaluated using the gas-phase theory that does not take into account condensed matter effects, viz. description of the electron wave function as a Bloch wave and modification of the electron−molecule interaction due to the polarization interaction of the surrounding medium.[38]

Figure 4 indicates that the charge trapping cross section is saturated beyond 8 ML thickness. In the vicinity of the metal substrate, however, we expect the transient anion to experience the increase in polarization due to the metal which further increases the survival probability factor. The higher magnitude of this factor should increase μ_0, but there are phenomena that adversely contribute to this cross section, the most prominent being the long-range interaction of incident electrons with the metal. In this energy range the electron wavelength compares with that of the Kr spacer thickness. Hence, at small L, electrons also interact with the large density of electronic states in the metal. This contributes to an increase in the final states of scattering and a decrease of the probability of electron interaction with the molecule, thereby reducing the cross section for electron capture and subsequently DA.[7] At larger L, the Kr spacer effectively shields the direct electron interaction with the metal. When the CF_3Cl-doped surface is sufficiently far away from the metal, the Kr surface polarization becomes the major factor that affects the fate of the transient anion. For negative ion resonances close to the metal, the anion's lifetime can also be reduced due to increased coupling between the wave functions of anion's image charge and that of the anion, thus allowing decay via electron tunneling to metal states above the Fermi level. This effect, however, becomes important only for $L < 2$ ML. Similar data have been reported for CH_3Cl.[7]

The low-energy resonance is considerably shifted to higher energies in the desorption yield as compared to its energy in the charge trapping cross section (Figure 2). This is due to the polarization barrier for the escaping Cl^- fragments. Only transitions at the high-energy tail of the condensed-phase resonance create Cl^- ions with sufficient kinetic energy to overcome that barrier. The low desorption intensity strongly indicates that the direct desorption processes do not take place to any appreciable extent. From the primary electron intensity, the density of the molecules at the surface, and the intensity of desorbed ions, we roughly estimate the Cl^- desorption cross section to be $\leq 10^{-23}$ cm^2.

For the low-energy condensed-phase single particle resonance, we have the following reaction channels:

$$CF_3Cl^-_{(ad)} \rightarrow CF_{3(ad)} + Cl^-_{(ad)} \quad (6a)$$

$$\rightarrow CF_3Cl^-_{(ad)} + \text{energy} \quad (6b)$$

$$\rightarrow CF_{3(g)} + Cl^-_{(ad)} \quad (6c)$$

$$\rightarrow CF_{3(ad)} + Cl^-_{(g)} \quad (6d)$$

$$\rightarrow CF_{3(g)} + Cl^-_{(g)} \quad (6e)$$

Channels 6a−6c contribute to charge accumulation with a cross section of 43×10^{-18} cm^2 as derived in the present work. Within the competing desorption channels 6c−6e, channel 6c with the charge remaining at the surface is the energetically most favorable one.

If a considerable amount of molecules is oriented with C−Cl axis pointing toward the surface, one expects a substantial higher cross section for the desorption channel 6c as compared to channels 6d and 6e which contribute to the Cl^- intensity in Figure 2a. Combined charge trapping and desorption measurements on the present or similar systems may hence represent good candidates to study desorption of neutral fragments induced by DA. The information thus obtained could be supplemented by investigating the branching ratio of the final states in condensed-phase DA experiments.

In summary, the interaction of electrons in the energy range from near zero to 10 eV with a submonolayer of CF_3Cl on a Kr film surface leads to the desorption of Cl^- and F^- fragment ions. The resonant nature of the desorption cross sections indicates that the processes are driven by DA. While Cl^- appears from resonances near 2 and 9.5 eV, the F^- feature peaks at 5.5 eV with a continuous increase of the intensity above 10 eV due to dipolar dissociation. These structures in the desorption yield are correlated to DA resonances observed in previous gas-phase experiments. Desorption from the strongly C−Cl repulsive single particle resonance is surprisingly weak, suggesting strong postdissociation interactions prior to desorption. Charge trapping is essentially restricted to the low-energy single particle resonance which is downshifted by more than 1 eV with respect to the gas-phase position at 2.0 eV. The trapping cross section is 43×10^{-18} cm^2, more than 1 order of magnitude higher than the gas-phase DA cross section. The data are reproduced fairly well by a semiclassical model.

Acknowledgment. This work was supported by the Deutsche Forschungsgemeinschaft, the Fonds der Chemischen Industrie, and the Medical Research Council of Canada. F.W. thanks the NATO for a traveling grant.

References and Notes

(1) Sanche, L.; Dechênes, M. *Phys. Rev. Lett.* **1988**, *61*, 2096.
(2) Sambe, H.; Ramaker, D. E.; Dechênes, M.; Bass, A. D. and Sanche, L. *Phys. Rev. Lett.* **1990**, *64*, 523.
(3) Sanche, L. In *Excess Electrons in Dielectric Media;* Ferradini, C., Jay-Gerin, J. P., Eds.; CRC Press: Boca Raton, FL, 1991.
(4) Michels, H. H. *Adv. Chem. Phys.* **1981**, *45*, 225.
(5) Schulz, G. J. *Rev. Mod. Phys.* **1973**, *45*, 423.
(6) Ayotte, P.; Gamache, J.; Bass, A. D.; Fabrikant, I. I.; Sanche, L. *J. Chem. Phys.* **1997**, *106*, 749.

(7) Sanche, L.; Bass, A. D.; Ayotte, P.; Fabrikant, I. I. *Phys. Rev. Lett.* **1995**, *75*, 3568.
(8) Jones, R. K. *J. Chem. Phys.* **1986**, *84*, 813.
(9) Mann, A.; Linder, F. *J. Phys. B: At. Mol. Opt. Phys.* **1992**, *25*, 1621.
(10) Illenberger, E.; Scheunemann, H.-U.; Baumgärtel, H. *Chem. Phys.* **1979**, *37*, 21.
(11) Hahndorf, I.; Illenberger, E.; Lehr, L.; Manz, J. *Chem. Phys. Lett.* **1994**, *231*, 460.
(12) Illenberger, E. *Ber. Bunsen-Ges. Phys. Chem.* **1982**, 86, 252.
(13) Illenberger, E. *Chem. Phys. Lett.* **1981**, *80*, 153.
(14) Underwood-Lemons, T.; Gergel, T. J.; Moore, J. H. *J. Chem. Phys.* **1995**, *102*, 119.
(15) Lehr, L.; Miller, W. H. *Chem. Phys. Lett.* **1996**, *250*, 512.
(16) Oster, T.; Ingólfsson, O.; Meinke, M.; Jaffke, T.; Illenberger, E. *J. Chem. Phys.* **1993**, *99*, 5141.
(17) Meinke, M.; Illenberger, E. *J. Phys. Chem.* **1994**, *98*, 6601.
(18) Stamatovic, A.; Schultz, G. J. *Rev. Sci. Instrum.* **1970**, *41*, 423.
(19) Marsolais, R. M.; Dechênes, M.; Sanche, L. *Rev. Sci. Instrum.* **1989**, *60*, 2724. Nagesha, K.; Gamache, J.; Bass A. D.; Sanche, L. *Rev. Sci. Instrum.* **1997**, *68*, 3883.
(20) Perluzzo, G.; Sanche, L.; Gaubert, C.; Baudoing, R. *Phys. Rev. B* **1984**, *30*, 4292.
(21) Schwentner, N.; Koch E.-E.; Jortner, J. *Springer Tracts Mod. Phys.* **1985**, *107*, 39.
(22) Ingólfsson, O., Weik, F.; Illenberger, E. *Int. J. Mass Spectrom. Ion Process* **1996**, *155*, 1.
(23) Verhaart, G. J.; Van der Hart, W. J.; Brongersma, H. H. *Chem. Phys.* **1978**, *34*, 161.
(24) Burton, K. J.; Wheaton, G. A. *J. Am. Chem. Soc.* **1974**, *21*, 6787.
(25) Jochims, H. W.; Lohr, W.; Baumgärtel, H. *Ber. Bunsen-Ges. Phys. Chem.* **1976**, *80*, 130.
(26) Doucet, J.; Sauvageau, P.; Sandorfy, C. *J. Chem. Phys.* **1973**, *58*, 3708.
(27) Weik, F.; Illenberger, E. *J. Chem. Phys.* **1995**, *103*, 1406.
(28) Michaud, M.; Sanche, L. *J. Electron Spectrosc. Relat. Phenom.* **1990**, *51*, 237.
(29) Nagesha, K.; Sanche, L. *Phys. Rev. Lett.* **1997**, *78*, 4725.
(30) O'Malley, T. F. *Phys. Rev.* **1966**, *150*, 14.
(31) Domcke, W. *Phys. Rep.* **1991**, *208*, 97.
(32) Lehr, L. Doctoral Thesis, Fachbereich Chemie, Freie Universität Berlin, 1996.
(33) Miller, W. H. J. *Chem. Phys.* **1970**, *52*, 3563.
(34) Read, F. H. *J. Phys.* **1968**, *31*, 893.
(35) Taylor, H. S. In *Advances in Chemical Physics*; Prigogine, I., Rice, S. A., Eds.; Interscience Publishers: New York, 1970; Vol. XVIII.
(36) Wigner, E. P. *Phys. Rev.* **1948,** *73*, 1002.
(37) Chutjian, A.; Alajajian, S. H. *Phys. Rev A* **1985,** *31*, 2885. Chutjian, A. *J. Phys. Chem.* **1982**, *86*, 3518.
(38) Fabrikant, I. I.; Nagesha, K.; Wilde, R.; Sanche, L. *Phys. Rev. B* **1997,** *56*, R5725.